

Effects of ion pairs on the dynamics of erbium-doped fiber lasers

François Sanchez

*Ecole Nationale Supérieure de Sciences Appliquées et de Technologie, Laboratoire d'Optronique,
6, Rue de Kerampont, 22305 Lannion, France*

Patrice Le Boudec and Pierre-Luc François

*France Telecom, Centre National d'Etudes des Telecommunications Lannion B, Fonctions Optiques Guidées,
Route de Tregastel, 22301 Lannion CEDEX, France*

Guy Stephan

*Ecole Nationale Supérieure de Sciences Appliquées et de Technologie, Laboratoire d'Optronique,
6, Rue de Kerampont, 22305 Lannion, France*

(Received 10 March 1993)

Experiments with erbium-doped fiber lasers demonstrate cw, sinusoidal, and self-pulsing operation. The obtained regimes depend on three control parameters: ion-pair concentration, photon lifetime, and pumping rate. We present a theoretical model which describes the active medium as a mixture of isolated ions and ion pairs. Starting with the adapted laser rate equations we show that the description of the dynamical behavior of this system can be reduced to only four first-order coupled equations. A linear stability analysis demonstrates the existence of self-pulsing for a finite range of pumping rates. At both ends of this range Hopf bifurcations occur: one located near the first laser threshold and the other at a higher pumping ratio, whose position is closely related to the pair concentration. Results of numerical calculations are in good qualitative agreement with our experimental data.

PACS number(s): 42.60.Mi, 42.55.-f, 42.50.Lc, 42.50.Fx

I. INTRODUCTION

Since the experimental observation of a train of undamped oscillations in the ruby laser [1], the dynamics of lasers has been a stimulating field of investigation [2–5]. Recently, the field of nonlinear instabilities has grown and attracted the attention of numerous workers [6]. In particular, self-pulsing in lasers has been the subject of intensive research [7]. Different physical origins have been experimentally demonstrated in several self-pulsing laser systems. It is well known that self-pulsing can be achieved in any laser with an adequate saturable absorber [8]. A more interesting case is when the laser itself delivers an infinite train of pulses, as is the case, for example, for the xenon laser [9], where the pulses are interpreted as an intrinsic instability of the cw solutions of the laser equations [10].

We have recently reported the experimental observation of self-pulsing in erbium-doped fiber lasers [11]. In the simplest experimental configuration (two-mirror cavity), the erbium-doped fiber laser (EDFL) operates with $\lambda = 1.55 \mu\text{m}$, in self-pulsing or in a cw mode for pumping wavelengths of 514.5, 810, or 980 nm [11–13]. Different hypotheses have been proposed in [11] to explain this instability. Our experimental work led us to attribute this behavior to the existence of ion pairs (or clusters), distributed within the fiber, which act as a saturable absorber [12].

Great interest was recently focused on ion interactions in rare-earth-element-doped fiber or crystals [14–18]. As the ion concentration is increased, the average distance between ions decreases, which enhances ion-ion interac-

tions. Such interactions can occur among all the ions in a fiber or only within a certain class of ions. Moreover, two or more ions can interact, leading to several cross-relaxation processes. For example, energy transfer between two adjacent ions (ion pair) has been successfully used to obtain laser emission in doped crystals via an up-conversion process [18]. In such cases it is important to control the fabrication process in order to obtain a high ion-pair concentration. The ion pairs can also involve two different dopants. Codoping of silicate fibers, for example, was also used to obtain a laser effect via energy transfer [14]. Nevertheless, although the previous examples show that ion pairs are sometimes needed, there are cases where their presence degrades the operating performance of a device. Indeed, the presence of such pairs has been identified as one important physical process which can limit the gain in erbium-doped fiber amplifiers at $1.55 \mu\text{m}$ [16]. Moreover, in erbium-doped fiber lasers, this phenomenon leads to both a reduction of the laser efficiency and an increase in laser threshold [17].

The aim of this paper is to develop a theoretical model describing the main features observed in EDFL. We assume that there exist only two classes of ions: (i) isolated ions and (ii) ion pairs. We demonstrate theoretically that the quenching process associated with ion pairs can drastically change the dynamical behavior of a laser: without pairs, the laser operates in cw regime, while their presence can lead to a self-pulsing instability. Section II presents a summary of our experimental results obtained with various EDFL's. In particular, the influence of the ion-pair concentration, the photon lifetime, and the pumping ratio are discussed. Section III is devoted to the

construction of a simple theoretical model which describes the different behaviors observed experimentally, depending on the ion-pair concentration. The isolated ion is described as a two-level system and the ion pair as a three-level system. In its simplest form, the model includes four coupled first-order differential equations: (i) one for the isolated ions, (ii) two for the ion pairs, and (iii) one for the laser field intensity. The stationary state is derived in Sec. IV where we present the influence of the ion pairs on both the laser output versus pumping ratio and laser threshold. In Sec. V we perform a linear stability analysis of the equations, which points out the emergence of a self-pulsing instability through a Hopf bifurcation. A numerical resolution of the equations is made in Sec. VI. Both the asymptotic regime and the transient evolution are investigated. In particular, we present a stability diagram as a function of the ion-pair concentration. Theoretical results are compared with experiments throughout the paper.

II. EXPERIMENTAL RESULTS

In this section, the experimental results obtained with various erbium-doped fiber lasers are summarized [11,12]. Several erbium-doped fibers have been used, their main difference being the ion-pair concentration x . This concentration has been measured by a pump-transmission method [21]. In our case, x varies from 0.008 to 0.23. A schematic view of the experimental setup is shown in Fig. 1. A laser is used to optically pump an Er^{3+} -doped optical fiber inside a two-mirror cavity (reflection coefficients $R_1=100\%$, $R_2=80\%$). The doped fibers had lengths between 3 and 6 m and were single mode at $\lambda=1.55 \mu\text{m}$. The pump lasers were (i) a cw argon-ion laser operating at 514.5 nm, (ii) a cw titanium:sapphire laser operating at 810 or 980 nm. The pump is time modulated by a chopper ($f=10 \text{ Hz}$) in order to observe the transient regime. A dispersive prism is placed inside the cavity allowing a spectral narrowing of the laser linewidth, together with a spectral tunability. The laser output around $1.55 \mu\text{m}$ is incident on a high-speed germanium photodiode (2 GHz). The signal is stored in a numerical oscilloscope and then transferred to a computer.

Figure 2 represents the energy levels of Er^{3+} . At $1.55 \mu\text{m}$, Er^{3+} operates as a three-level system. The low level of the lasing transition is the ground state, which makes it necessary to optimize the fiber length [19] in order to

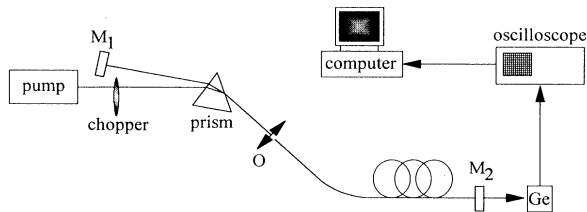


FIG. 1. Schematic representation of the experimental setup: the pump laser is injected via the microscope objective O . The laser oscillation is obtained between M_1 ($R_1=100\%$) and M_2 ($R_2=80\%$).

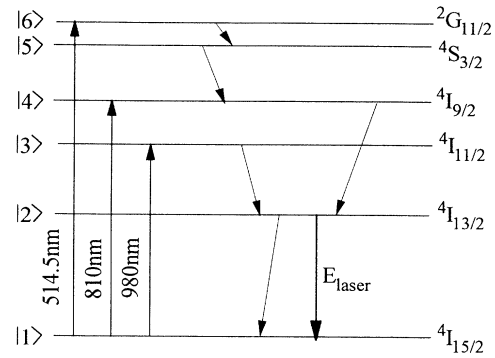


FIG. 2. Energy levels of Er^{3+} showing the lasing transition, the pumping levels, and the relaxation processes.

avoid too much reabsorption of the laser signal along the propagation axis. Note that a quasisonance at the lasing wavelength occurs between levels $4I_{13/2}$ and $4I_{9/2}$ [20].

In [11] we have reported that, for a fiber having an ion-pair concentration of about $x=0.18$, self-pulsing occurs for any pumping ratio and for any of the pump wavelengths mentioned above. Figure 3 gives an example of such pulses obtained with this fiber in the cavity configuration of Fig. 1. The period of the pulses is a decreasing function of pumping ratio r , varying between 80 and $30 \mu\text{s}$ when r changes from 1.1 to 2.3 as shown in Fig. 4. The pulse width decreases from about 20 to $5 \mu\text{s}$ when r increases. In addition, a modification of the dynamics appears when the oscillation is obtained between the output mirror and the 4% Fresnel reflection at the fiber end face located near the prism ("bad"-cavity configuration). In such conditions, the output intensity is quasistationary near threshold and becomes self-pulsing for higher pumping ratios.

More recently [12], we have reported the experimental influence of ion-pair concentration on the dynamics of erbium-doped fiber lasers. In particular, we have demonstrated that for $x \leq 0.06$ the output intensity is cw for any pumping ratio. Around $x \approx 0.075$ the output intensity varies continuously from self-pulsing to cw when r is increased. For higher pair concentrations ($x \geq 0.10$), the

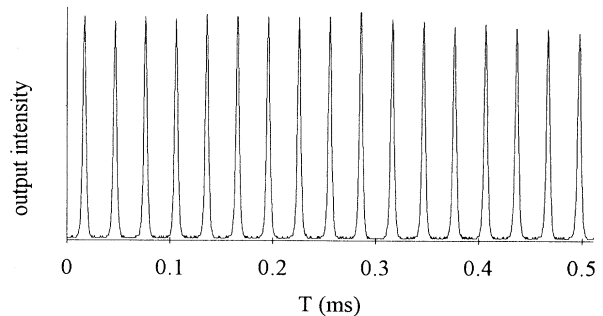


FIG. 3. Self-pulsing output of the erbium-doped fiber laser for a pumping ratio $r=2.3$. The fiber used had a pair concentration $x=0.18$, a length $l=3 \text{ m}$, and was pumped at 810 nm.

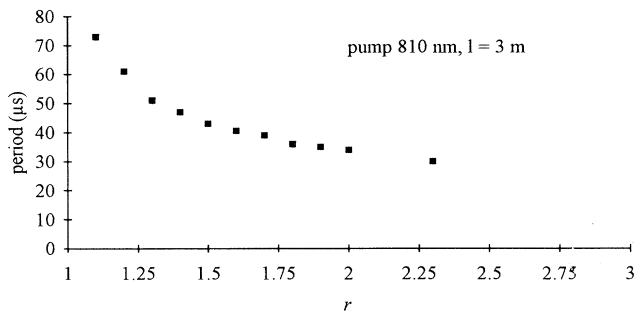


FIG. 4. Experimental evolution of the pulse period vs r . The fiber was used in the experimental setup of Fig. 1 and pumped at 810 nm. The pair concentration is $x = 0.18$ and the length $l = 3$ m.

laser is self-pulsing for any of the pumping rates used; we expect that a cw operation can be obtained for higher pumping rates not achievable in our experiments. Figure 5 shows typical output signals observed for $x = 0.075$ for three pumping ratios, in the experimental configuration of Fig. 1: the laser evolves from self-pulsing to a

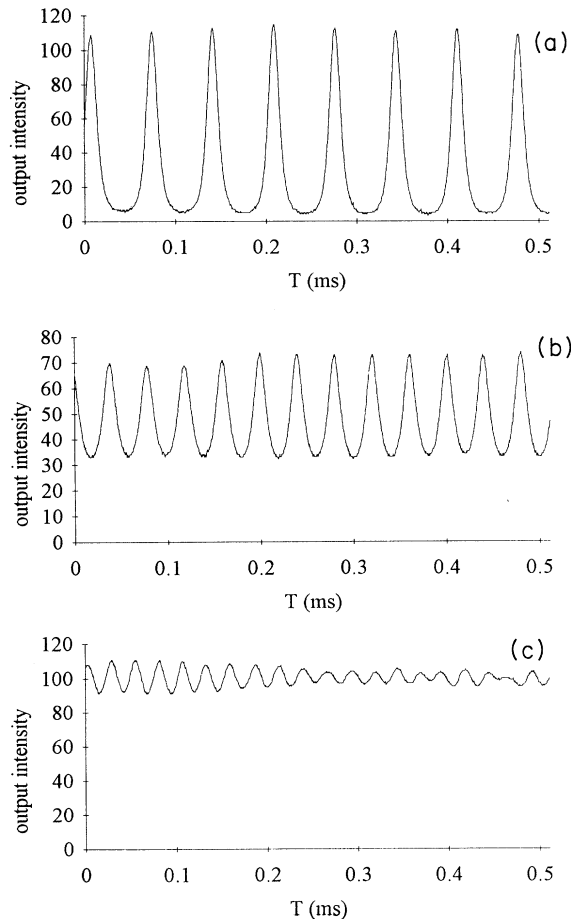


FIG. 5. Dynamical behavior of a 5-m EDFL pumped at $\lambda_p = 810$ nm for a pair concentration $x = 0.075$: (a) self-pulsing occurs for $r = 2$, (b) a sinusoidal output arises for $r = 4$, and (c) a cw output establishes for $r = 5$.

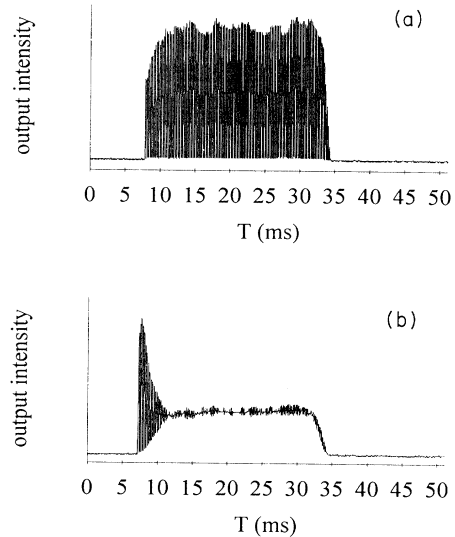


FIG. 6. Transient behavior of a 5-m erbium-doped fiber laser with $x = 0.075$: (a) $r = 3.5$, (b) $r = 5.0$ ($\lambda_p = 810$ nm).

sinusoidal output and then to a cw operation when increasing the pumping ratio.

The transient regimes leading to these self-pulsing, sinusoidal, or cw operations are also very different. This is clearly seen in Fig. 6, which gives examples of the transient behavior of a doped fiber laser for different pumping rates. The ion-pair concentration of the fiber used is $x = 0.075$. For a self-pulsing regime, the transient evolution is a succession of increasing pulses as is shown in Fig. 6(a). When the laser evolves to a cw operation as in Fig. 6(b), the transient behavior corresponds to classical relaxation oscillations similar to those observed in Nd^{3+} -doped fiber laser [22]. In a bad-cavity configuration, the transient behavior is analogous to that shown in Fig. 7, obtained near laser threshold (in this case $x = 0.23$).

III. CONSTRUCTION OF THE MODEL

Our experimental results prove that the dynamics of the EDFL is strongly dependent on the ion-pair concentration. In this section we develop a model which takes into account the existence of both these ion pairs (proportion x) and isolated ions (proportion $1 - 2x$). The laser

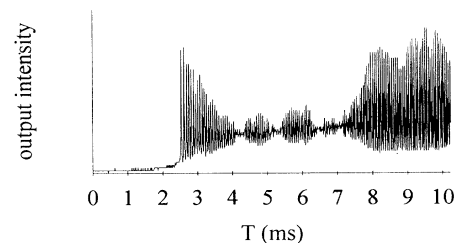


FIG. 7. Transient behavior in a bad-cavity configuration for $x = 0.23$ and $r = 1.1$ ($l = 6$ m and $\lambda_p = 810$ nm).

field interacts with both of these atomic systems. The difficulty is to model the energy levels of an ion pair. This problem is similar to the construction of molecular states starting with individual atomic states, but may be simplified by considering the physical processes which have been observed in ion pairs [16,17].

A. Isolated ion

The laser transition occurs between the ${}^4I_{13/2}$ and ${}^4I_{15/2}$ levels of Fig. 2. Nevertheless, it is important to stress that a quasiresonance occurs between level ${}^4I_{9/2}$ and level ${}^4I_{13/2}$ for the lasing wavelength. For convenience and simplicity, we consider here the isolated ion as the two-level system shown in Fig. 8.

B. Ion pair

A consequence of the ion-pair interaction is the cross-relaxation process [16,17]. Such a process involves two neighboring ions in the ${}^4I_{13/2}$ state: one of the ions transfers its energy to the other, producing one up-converted ${}^4I_{9/2}$ ion and one ground-state ion (Fig. 9). The characteristic time associated with this process is estimated to be between 1 and 10 μs [21]. The up-converted ion quickly decays to the ${}^4I_{13/2}$ state. The consequence is the loss of one excited erbium ion. This effect is responsible for the limitation of the gain in erbium-doped fiber amplifiers [16]. Thus, in a simple approach, the ion pair can be described by the interaction of two three-level ions: (${}^4I_{15/2}$, ${}^4I_{13/2}$, ${}^4I_{9/2}$).

The aim in this section is to find the eigenstates of an ion pair. The treatment of such a problem is, in general, complicated, and one needs to solve the Schrödinger equation where the Hamiltonian takes into account the interaction of the two ions. We do not use such an exact approach in this paper. In order to achieve a simple description of the problem, we assume that the atomic state of an ion pair can be written as (α, β) where α and β are the states of the two isolated ions. This approach neglects the interaction energy of the two ions, which is justified by the screening effect of the $4d^{10}$ electrons on the active $4f$ electrons [23]. Such a screening prevents a significant modification of the energy levels of a rare-earth ion in a given host, while permitting considerable variations of transition probabilities. In these conditions the energy of a pair is merely the sum of the energy of the

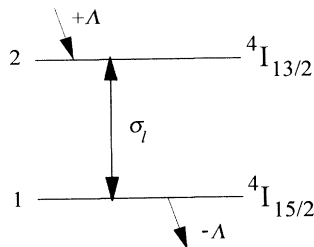


FIG. 8. Energy diagram used for the description of an isolated ion. Λ is the pumping rate and σ_i the absorption cross section.

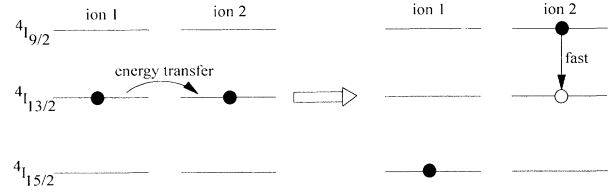


FIG. 9. Up-conversion process in ion pairs.

two ions. Starting from the three-level scheme for an isolated ion (${}^4I_{15/2}$, ${}^4I_{13/2}$, ${}^4I_{9/2}$), it is then possible to build the six different energy levels for a pair, indicated in Fig. 10(a). It is interesting to note that in this energy diagram, levels $|22\rangle$ and $|13\rangle$ are very close to one another and thus the coupling between these two states is strong. A consequence is a fast nonradiative relaxation from state $|22\rangle$ to state $|13\rangle$ ($\tau=1$ to $10 \mu\text{s}$) [21]. In this relaxation process, the population inversion decreases with no contribution to the laser field. Then level $|13\rangle$ quickly relaxes to level $|12\rangle$ [20].

The states $|33\rangle$, $|23\rangle$, and $|13\rangle$ all contain the ${}^4I_{9/2}$ level which relaxes faster than level ${}^4I_{13/2}$. As a conse-

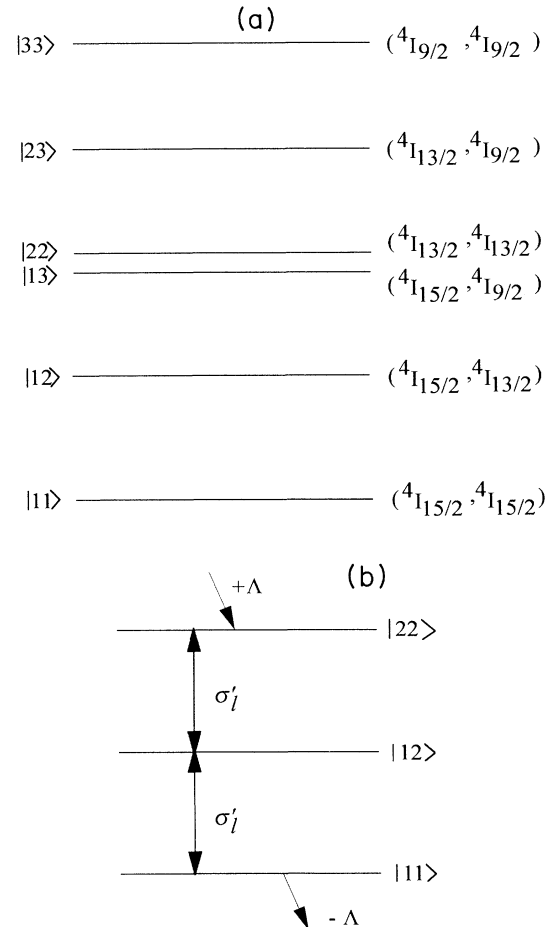


FIG. 10. (a) Energy diagram for an ion pair. (b) Simplified energy diagram used in this model.

quence, it is thus possible to neglect the population of these combined states when compared to that of levels $|11\rangle$, $|12\rangle$, and $|22\rangle$, which involve the ground state and the metastable ${}^4I_{13/2}$ state. According to both the two-level approach for an isolated ion and the small lifetime of ion-pair levels including the ${}^4I_{9/2}$ state, we describe an ion pair as a three-level system: (${}^4I_{15/2}$, ${}^4I_{15/2}$), (${}^4I_{15/2}$, ${}^4I_{13/2}$), and (${}^4I_{13/2}$, ${}^4I_{13/2}$) [Fig. 10(b)]. In such an approach, the ion pair presents two resonant transitions for the laser field near $\lambda=1.55\ \mu\text{m}$. We assume here that the lifetime of $|12\rangle$ is the same as that of ${}^4I_{13/2}$ for the isolated ion (10 ms). Due to the fast relaxation of $|13\rangle$ to $|12\rangle$, the relaxation time from $|22\rangle$ to $|12\rangle$ will be assumed to be between 1 and 10 μs (relaxation time from $|22\rangle$ to $|13\rangle$). We assume moreover that the absorption cross sections around $\lambda=1.55\ \mu\text{m}$ for the two resonant transitions are the same but are different from that of an isolated ion.

C. Material and field equations

This model is based on the rate equations because of the fast relaxation time associated with the electronic polarizations (large homogeneous broadening due to collisions with phonons) [24]. The dynamical behavior of an isolated ion is described by the following rate equations:

$$\begin{aligned}\frac{dn_1}{dt} &= -\Lambda + a_2 n_2 + i_l (n_2 - n_1), \\ \frac{dn_2}{dt} &= \Lambda - a_2 n_2 - i_l (n_2 - n_1),\end{aligned}\quad (1)$$

where $a_2 = \gamma_2 / \gamma_l$; $n_{1,2} = N_{1,2} / (1-2x)N_0$; and $i_l = \sigma_l I_l / \gamma_l$; $N_{1,2}$ is the population of level 1 or 2 with $N_1 + N_2 = (1-2x)N_0$; N_0 is the erbium concentration; γ_2 and γ_l are the relaxation rates, respectively, of the upper level of the laser transition and of the laser field; σ_l is the absorption cross section for the isolated ion; I_l is the photon flux of the laser field and Λ is the pumping rate. The time is normalized with respect to the photon lifetime $\tau_l = 1/\gamma_l$.

In terms of the normalized population inversion $n_i = n_2 - n_1$, the evolution of the system is described by the following equation:

$$\frac{dn_i}{dt} = 2\Lambda - a_2(1+n_i) - 2i_l n_i. \quad (2)$$

According to the three-level scheme adopted for the ion pairs, the corresponding dynamical behavior is described by the following three rate equations:

$$\begin{aligned}\frac{dn_{11}}{dt} &= -\Lambda + a_{12}n_{12} + y_i(n_{12} - n_{11}), \\ \frac{dn_{12}}{dt} &= -a_{12}n_{12} + a_{22}n_{22} - y_i(n_{12} - n_{11}) \\ &\quad + y_i(n_{22} - n_{12}), \\ \frac{dn_{22}}{dt} &= \Lambda - a_{22}n_{22} - y_i(n_{22} - n_{12}),\end{aligned}\quad (3)$$

with $y = \sigma'_l / \sigma_l$ where σ'_l is the absorption cross section at the lasing wavelength for a pair, with $a_{ij} = \gamma_{ij} / \gamma_l$ where γ_{ij} is the relaxation rate of level $|ij\rangle$ and $n_{ij} = N_{ij} / xN_0$, with our normalization $n_{11} + n_{12} + n_{22} = 1$.

With the new variables $n_+ = n_{22} + n_{11}$ and $n_- = n_{22} - n_{11}$, the system is reduced to the two following equations:

$$\begin{aligned}\frac{dn_+}{dt} &= a_{12}(1-n_+) - \frac{a_{22}}{2}(n_+ + n_-) + y_i(2-3n_+), \\ \frac{dn_-}{dt} &= 2\Lambda - a_{12}(1-n_+) - \frac{a_{22}}{2}(n_+ + n_-) - y_i n_-.\end{aligned}\quad (4)$$

The laser field interacts with two systems: (i) the fraction $1-2x$ of isolated ions and (ii) the fraction x of ion pairs. The dynamics of the laser intensity can therefore be written as

$$\frac{di_l}{dt} = -i_l + (1-2x)A i_l n_i + xB i_l n_-, \quad (5)$$

with $A = \sigma_l N_0 / \gamma_l$; $B = \sigma'_l N_0 / \gamma_l$. One notes that $y = B/A$.

In summary, with the simple approach adopted here, the dynamical behavior of the system is described using only the following four coupled first-order differential equations:

$$\frac{dn_i}{dt} = 2\Lambda - a_2(1+n_i) - 2i_l n_i, \quad (6a)$$

$$\frac{dn_+}{dt} = a_{12}(1-n_+) - \frac{a_{22}}{2}(n_+ + n_-) + y_i(2-3n_+), \quad (6b)$$

$$\frac{dn_-}{dt} = 2\Lambda - a_{12}(1-n_+) - \frac{a_{22}}{2}(n_+ + n_-) - y_i n_-, \quad (6c)$$

$$\frac{di_l}{dt} = -i_l + (1-2x)A i_l n_i + xB i_l n_-. \quad (6d)$$

IV. STEADY STATE

The populations at steady state can easily be expressed with respect to the steady-state laser intensity using relations (6a), (6c), and (6d):

$$\begin{aligned}\bar{n}_i &= \frac{2\Lambda - a_2}{a_2 + 2\bar{i}_l}, \\ \bar{n}_- &= \frac{1 - A(1-2x)\bar{n}_i}{xB}, \\ \bar{n}_+ &= -\frac{2\Lambda - a_{12}}{a_{12} - a_{22}/2} + \frac{y\bar{i}_l + a_{22}/2}{a_{12} - a_{22}/2} \bar{n}_-.\end{aligned}\quad (7)$$

Combining relations (6b) and (7) allows us to obtain a third-order polynomial equation for the steady-state laser intensity:

$$\begin{aligned}
& \bar{i}_l^3 \left[-\frac{6y}{A} \right] + \bar{i}_l^2 y \left[-2x(a_{12} + a_{22} - 3a_2) - \frac{1}{B}(2a_{12} + 4a_{22} + 3ya_2) + 3(2\Lambda - a_2) \right] \\
& + \bar{i}_l \left[2x(a_{12} - \frac{1}{2}a_{22})(a_{12} + ya_2) - \frac{1}{B}(2a_{22}a_{12} + 2ya_2a_{22} + ya_{12}a_2) \right. \\
& \quad \left. + x(2a_{12} + a_{22} + 3ya_2)(2\Lambda - a_{12}) + (a_{12} + 2a_{22})(1 - 2x)(2\Lambda - a_2) \right] \\
& + \left[xa_2(-a_{22}a_{12} + 2\Lambda a_{12} + a_{22}\Lambda) - \frac{a_2a_{22}a_{12}}{B} + \frac{1}{y}a_{22}a_{12}(1 - 2x)(2\Lambda - a_2) \right] = 0. \quad (8)
\end{aligned}$$

For pumping rates greater than the laser threshold, relation (8) has only one real and positive root for the parameters used.

The laser threshold is obtained from relation (8) by taking the laser intensity equal to zero and solving for Λ :

$$\Lambda_{\text{th}} = \frac{a_2a_{22}a_{12}[x + (1 - 2x)/y + 1/B]}{xa_2(2a_{12} + a_{22}) + 2a_{12}a_{22}(1 - 2x)/y}. \quad (9)$$

In the particular case where $x = 0$, the threshold becomes

$$\Lambda_{\text{th}}^0 = \frac{a_2}{2} \left[1 + \frac{1}{A} \right], \quad (10)$$

which can also be obtained directly from (2) and (6d).

At this stage, it is interesting to compare the thresholds with and without ion pairs. To do this, we plot in Fig. 11 the ratio $\Lambda_{\text{th}}/\Lambda_{\text{th}}^0$ versus x for different photon lifetimes τ_l and for $y = 0.2$. In fact, the ratio y of the absorption cross sections for the pair and the solitary ion is unknown and thus can be considered as a fitting parameter. Figure 11 shows that the threshold is an increasing function of the ion-pair concentration x . Additionally, for a given x , the threshold increases with γ_l . Note that the influence of ion pairs on laser threshold is quite small for low x values.

Figure 12 shows the evolution of the steady-state laser

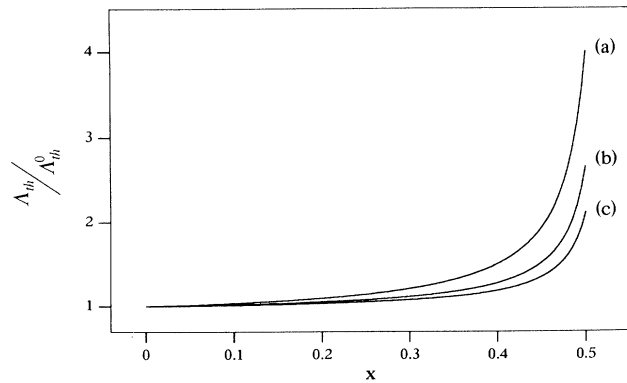


FIG. 11. Evolution of the threshold vs x for $y = 0.2$ and for different photon lifetimes: (a) $\gamma_l = 10^8 \text{ s}^{-1}$, (b) $\gamma_l = 3 \times 10^7 \text{ s}^{-1}$, and (c) $\gamma_l = 5 \times 10^6 \text{ s}^{-1}$.

intensity versus the pumping ratio $r = \Lambda/\Lambda_{\text{th}}$ for some x values. We see that the presence of ion pairs not only increases the pump power threshold, but also leads to a decrease in the slope of the characteristic, leading thus to a smaller efficiency.

V. LINEAR STABILITY ANALYSIS

We perform here a classical stability analysis of Eq. (6) around the steady state obtained from Eqs. (7) and (8). We consider small variations from steady state:

$$\delta = \begin{pmatrix} n_i - \bar{n}_i \\ n_+ - \bar{n}_+ \\ n_- - \bar{n}_- \\ i_l - \bar{i}_l \end{pmatrix}. \quad (11)$$

These variations evolve with time according to the system obtained from Eq. (6) linearized around its steady-state solution:

$$\frac{\partial \delta}{\partial t} = L \delta, \quad (12)$$

where

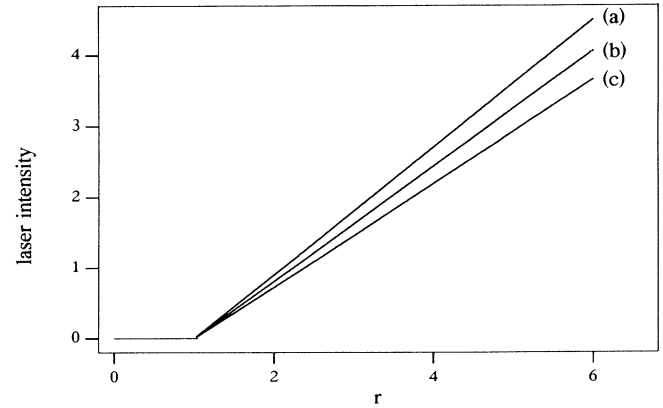


FIG. 12. Characteristic of the laser for different pair concentrations: (a) $x = 0$, (b) $x = 0.05$, and (c) $x = 0.10$. The parameters used are $\gamma_l = 10^8 \text{ s}^{-1}$ and $y = 0.2$.

$$L = \begin{pmatrix} -a_2 - 2\bar{i}_l & 0 & 0 & -2\bar{n}_l \\ 0 & -a_{12} - \frac{1}{2}a_{22} - 3y\bar{i}_l & -\frac{1}{2}a_{22} & y(2 - 3\bar{n}_+) \\ 0 & a_{12} - \frac{1}{2}a_{22} & -\frac{1}{2}a_{22} - y\bar{i}_l & -y\bar{n}_- \\ (1 - 2x)A\bar{i}_l & 0 & xB\bar{i}_l & 0 \end{pmatrix}. \quad (13)$$

System (12) can be solved by direct integration. The solutions are expressed as linear combinations of $\exp(\lambda_n t)$ terms, where λ_n is an eigenvalue of matrix L (Lyapunov exponent). The eigenvalues are calculated from the characteristic equation:

$$\det(L - \lambda I) = 0. \quad (14)$$

Among the four eigenvalues of system (12), two always remain real and negative, while the other two are complex conjugate and can have a positive real part. In Fig. 13(a) we show in the complex plane the two complex-conjugate eigenvalues obtained for r between 1 and 19. Curves are presented for the four x values indicated. One sees that for a high enough pair concentration (here $x > 0.05$), there exist r values leading to $\text{Re}(\lambda) > 0$. The crossing of the imaginary axis in such a way is characteristic of a Hopf bifurcation [25,26]. Figure 13(b) shows the evolution of $\text{Re}(\lambda)$ versus r . As expected, the r inter-

val where $\text{Re}(\lambda) > 0$ depends on the values of y and x . In particular the interval broadens when x increases. Near the bifurcation points, the eigenvalue is nearly pure imaginary, which corresponds to a sinusoidal laser output.

The previous results can be represented in a stability diagram which gives, for each x , the values of r for which the complex-conjugate eigenvalues cross the imaginary axis. This determines the stable or unstable character of the laser output. Figure 14(a) gives the theoretical stability diagram for different photon lifetimes and Fig. 14(b) gives the experimental diagram obtained from our results [12]. We see that this simple model leads to a good qualitative agreement. Further experimental work is needed to obtain a more precise bifurcation diagram for intermediate values of x . Figure 14(a) shows moreover that in a high loss cavity ($\gamma_l \geq 10^8 \text{ s}^{-1}$), the system is stable near the laser threshold, then becomes self-pulsing and finally stable again for increasing pumping rates. This behavior, near threshold, has been observed experimentally [11] when the oscillation is obtained by removing the M_1 mirror and using the fiber end as a mirror. The stability dia-

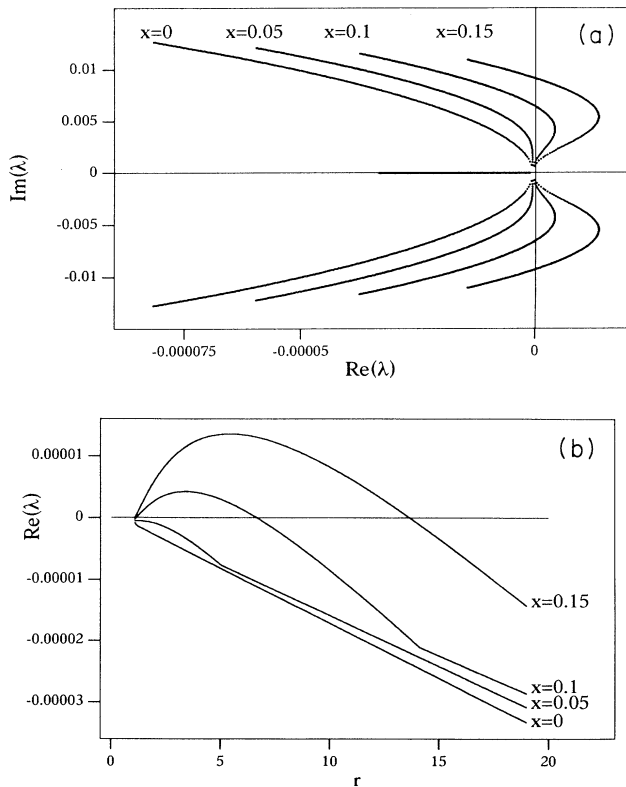


FIG. 13. (a) Evolution of the eigenvalues in the complex plane vs r . (b) Evolution of $\text{Re}(\lambda)$ vs the pumping ratio r . $\gamma_l = 1 \times 10^8 \text{ s}^{-1}$, $y = 0.2$.

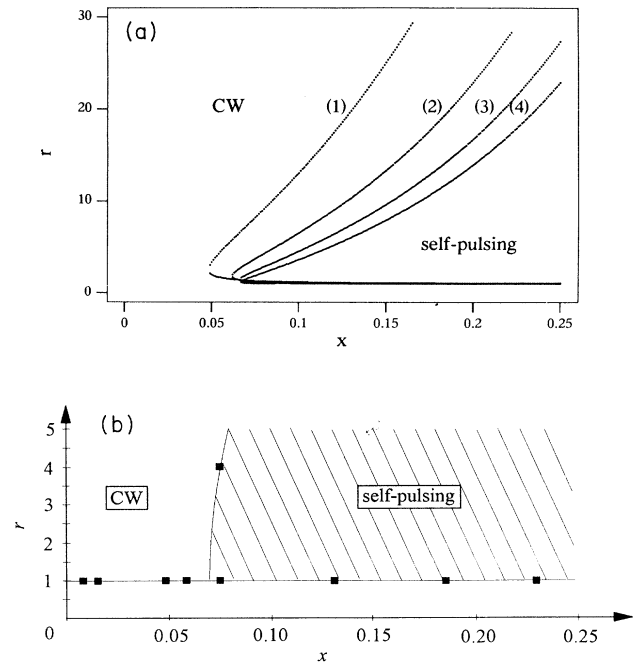


FIG. 14. (a) Theoretical stability diagram for different photon lifetimes and for $y = 0.2$: (1) $\gamma_l = 5 \times 10^8 \text{ s}^{-1}$, (2) $\gamma_l = 1 \times 10^8 \text{ s}^{-1}$, (3) $\gamma_l = 3 \times 10^7 \text{ s}^{-1}$, (4) $\gamma_l = 5 \times 10^6 \text{ s}^{-1}$. (b) Experimental stability diagram.

grams show also that the unstable zone depends on the photon lifetime: a bad cavity is a more favorable device to observe a self-pulsing oscillation.

We have also considered the influence of y on the stability of the system. For $y \approx 1$ the system is self-pulsing for a large range of pumping rates for $x \geq 0.001$. As this result does not correspond to the experimental data, we have considered smaller y values. On the opposite, for low y ($y \leq 0.1$), the system is stable for any r and x values. In this paper we have taken $y = 0.2$ in order to match the experimental x value beyond which the laser becomes self-pulsing.

VI. NUMERICAL CALCULATION

In this section, system (6) is solved numerically using a fifth-order Runge-Kutta method with an adaptive integration step. We are interested in both the asymptotic and the transient regimes. The physical parameters used for the numerical analysis are given in Table I [20,27].

A. Asymptotic regime

Figures 15(a)–15(c) show the theoretical time evolution of the laser intensity for increasing pumping rates in the case $x = 0.10$. Just above threshold (actually for $r \leq 1.14614$), the laser operates in cw mode. A Hopf bifurcation occurs when r is slightly increased: the system then delivers an infinite train of pulses. This behavior is observed from this critical pumping ratio up to $r = 6$ [see Figs. 15(a) and 15(b)]. Above this value, the output laser intensity becomes sinusoidal as shown in Fig. 15(c) (for $r = 6.656$). For slightly higher pumping ratios, the system becomes stable: a second Hopf bifurcation is localized near this value. This behavior is similar to that of a laser with a saturable absorber. In our case, the ion pairs act as a saturable absorber equally distributed along the optical fiber. The same kind of change in dynamics with the pumping ratio is obtained for any ion-pair concentration larger than $x \approx 0.06$. Beyond the second Hopf bifurcation, the upper ion-pair laser transition is saturated, thus leading to a stable cw operation. These numerical results confirm the predictions of the linear stability analysis. The comparison of Fig. 5 with Fig. 15 shows that the theoretical results are qualitatively in good agreement with the experimental data.

Figure 16 gives the theoretical evolution of the pulse period with the pumping ratio for the ion-pair concentrations $x = 0.08$ and 0.1 . The discontinuity in the curves indicates the transition between the cw and self-pulsing outputs. The period varies from some $100 \mu\text{s}$ near thresh-

old to about $20 \mu\text{s}$ for $r = 5$. These values are of the same order of magnitude as those measured experimentally [11,12]. Moreover, for a given pumping ratio, the period increases with x . The theoretical pulse width is a decreasing function of r as is observed experimentally [11], with typical values of some μs . It is important to note that near the first Hopf bifurcation the time evolution of the system is very slow and hence the asymptotic regime is achieved after a very-long-time transient regime.

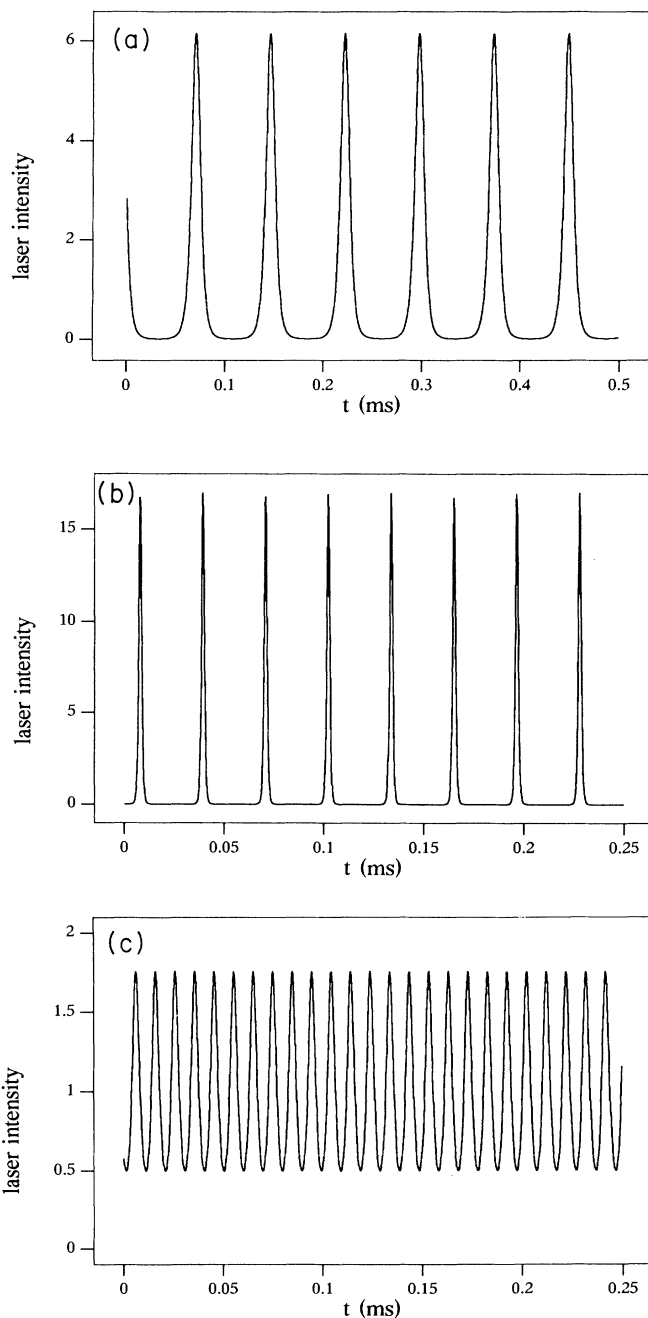


FIG. 15. Numerical solutions of system (9) with $y = 0.2$, $x = 0.1$, and $\gamma_l = 10^8 \text{ s}^{-1}$. (a) $r = 1.15$, (b) $r = 3$, and (c) $r = 6.656$.

TABLE I. Parameters used for the numerical calculation.

| | |
|-------------|---|
| τ_2 | 10 ms |
| τ_{22} | 2 μs |
| τ_{13} | 0.1 μs |
| τ_{12} | 10 ms |
| τ_1 | 2–200 ns |
| N_0 | $5 \times 10^{18} \text{ cm}^{-3}$ |
| σ_1 | $1.6 \times 10^{-10} \text{ cm}^3 \text{ s}^{-1}$ |
| y | 0.2 |

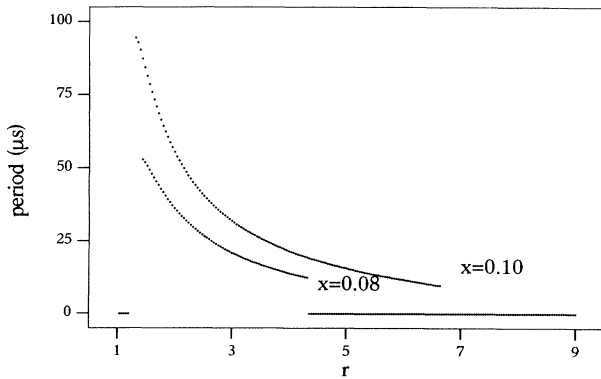


FIG. 16. Theoretical evolution of the period vs the pumping ratio with $y=0.2$ and $\gamma_l=1 \times 10^8 \text{ s}^{-1}$.

B. Transient regime

As shown in Figs. 6(a) and 6(b), the transient regimes leading to an unstable or stable cw state are very different. In order to make a complete comparison between our model and the experimental results, it is also necessary to consider the transient regime. Experimentally, when the laser is self-pulsing, the intensity of the

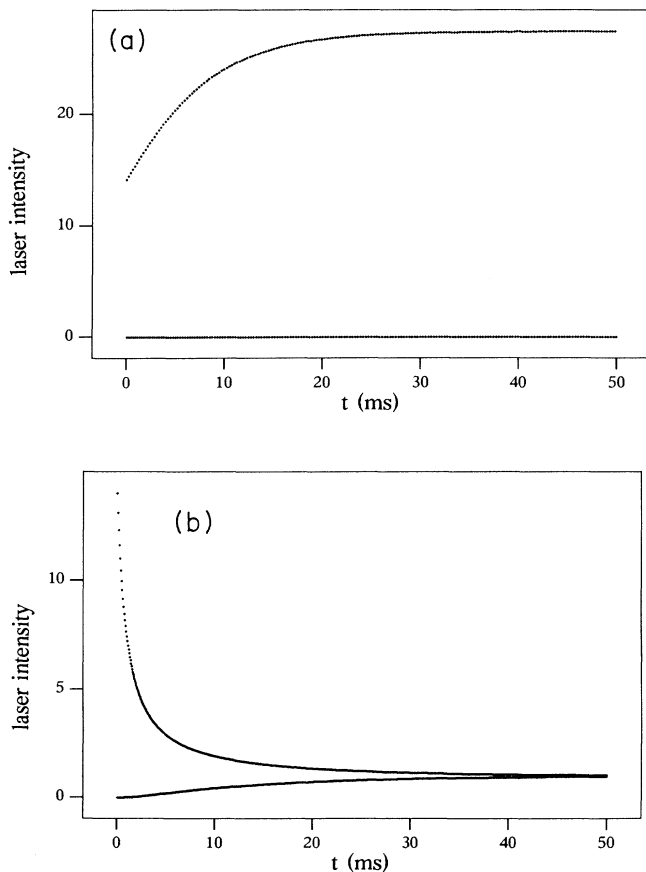


FIG. 17. Envelope of the theoretical transient of the laser intensity with $y=0.2$ and $x=0.10$: (a) $r=2$ and (b) $r=7$.

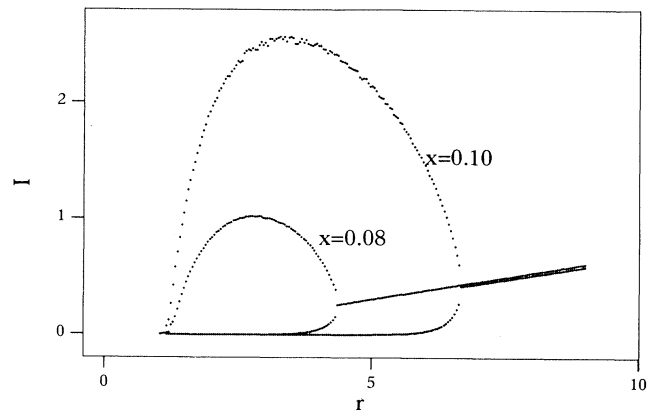


FIG. 18. Bifurcation diagram vs r for $y=0.2$ and $\gamma_l=1 \times 10^8 \text{ s}^{-1}$ for the x values indicated.

pulses increases and becomes stable after some ms, as shown in Fig. 6(a). This transient behavior is always observed in self-pulsing mode. On the contrary, the transient evolution towards the cw steady state corresponds to the classical relaxation oscillations [11,22] [Fig. 6(b)].

In order to obtain a clear theoretical figure, we have only plotted the extrema of the laser oscillations, i.e., the envelope of the laser intensity. The results are shown in Fig. 17 in the case where $x=0.1$. With this ion-pair concentration, our model exhibits both types of transient behaviors. For $r=2$ self-pulsing occurs with its characteristic transient, as shown in Fig. 17(a). For $r=7$, one obtains the classical relaxation oscillations leading to the cw operation, as shown in Fig. 17(b). These theoretical results are in good agreement with the experimental data shown in Fig. 6, which support the validity of our model.

C. Bifurcation diagrams

It is instructive to investigate the evolution of the pulse amplitude versus r . This evolution is usually represented as a bifurcation diagram which gives the maxima and minima of the laser signal as r is varied. Figure 18 gives the results of the numerical calculation for $x=0.08$ and 0.10 . Near the first laser threshold, the system is cw then a Hopf bifurcation appears for $r \approx 1.1$. The self-pulsing behavior occurs until $r=6.656$ for $x=0.10$, where the second Hopf bifurcation occurs. Note that this r value strongly increases with x . The system then exhibits cw operation for higher r values.

VII. CONCLUSIONS

This paper has been devoted to the study of dynamical behavior of erbium-doped fiber lasers. Different experiments conclusively show that the time evolution of the laser intensity depends on (i) the photon lifetime in the cavity, (ii) the pumping ratio, and (iii) the ion-pair concentration. In particular, self-pulsing operation was only observed in lasers with a large enough ion-pair concentration x . Moreover, for a given x which allows a dynamical instability, self-pulsing occurs for a finite range of pumping rates.

Our theory compares favorably with experiment. The

influence of the ion-pair concentration on the dynamical behavior of the EDFL is the same for both theory and experiment. The different transient behaviors observed in cw or self-pulsing operation have been obtained numerically. Nevertheless, further theoretical work is needed to achieve a more detailed agreement with experiment.

Our initial goal was not to develop a complete model but rather to propose a simple approach so as to gain some physical insight into the self-pulsing instability in EDFL. A more comprehensive description should take into account not only ion-pair interactions but also the interaction between more than two ions (clusters). Moreover, the eigenstates of ion clusters should be found with the quantum-mechanical theory. The difficulty here was to simplify the exact problem to allow an easy physical interpretation of the dynamics in order to obtain useful results and to focus on the main cause of the laser behavior: we have theoretically demonstrated that the existence of ion pairs is sufficient to explain the self-pulsing instability through a saturable-absorber mechanism. Nevertheless, the theoretical results do not imply that the ion-pair interactions are the only possible physical process responsible for the self-pulsing instability in erbium-

doped fiber lasers, but we have proved that they are a good candidate.

In summary, we have presented a theoretical model of a laser where the active medium is composed of both isolated ions and ion pairs. The numerical results are in good qualitative agreement with the experimental data obtained with various EDFL's. The model demonstrates that ion pairs are able to describe practically the whole range of dynamical behaviors observed. The concepts developed in this paper could certainly be used for other rare-earth ions, such as, for example, neodymium, where ion clusters can also be encountered.

ACKNOWLEDGMENTS

The experiments have been done with fibers fabricated by J. F. Bayon. One fiber was kindly provided by H. Fevrier from Alcatel. We thank E. Delevaque for measuring the ion-pair concentration in the fibers. We have benefited by discussions with M. Monerie and C. Vassallo from CNET. Thanks are due to K. Dworschak and B. Meziane for comments on the manuscript. The Laboratoire d'Optronique is "associée au CNRS (EP0001)."

-
- [1] T. H. Maiman, *Nature (London)* **187**, 493 (1960).
 - [2] R. Dunsmuir, *J. Electron. Control* **10**, 453 (1961).
 - [3] C. L. Tang, H. Statz, and G. De Mars, *J. Appl. Phys.* **34**, 2289 (1963).
 - [4] C. L. Tang, *J. Appl. Phys.* **34**, 2935 (1963).
 - [5] J. A. Fleck and R. E. Kidder, *J. Appl. Phys.* **35**, 2825 (1964).
 - [6] See, for example, the special issue on Nonlinear Laser Instabilities, *J. Opt. Soc. Am. B* **5**, No. 5 (1988).
 - [7] H. Risken and K. Nummedal, *J. Appl. Phys.* **39**, 4662 (1968); Hong Fu, *Phys. Rev. A* **40**, 1868 (1989); Hong Fu and H. Haken, *ibid.* **42**, 4151 (1990).
 - [8] T. Erneux, *J. Opt. Soc. Am. B* **5**, 1063 (1988).
 - [9] L. W. Casperson, *J. Opt. Soc. Am. B* **2**, 62 (1985); B. Meziane and H. Ladjouze, *Phys. Rev. A* **45**, 3150 (1992).
 - [10] H. Haken, *Phys. Lett.* **53A**, 77 (1975); C. Sparrow, *The Lorenz Equation: Bifurcation, Chaos and Strange Attractors*, Applied Mathematical Science Vol. 41 (Springer-Verlag, Heidelberg, 1982).
 - [11] P. Le Boudec, M. Le Flohic, P. L. Francois, F. Sanchez, and G. Stephan, *Opt. Quantum Electron.* **25**, 359 (1993).
 - [12] P. Le Boudec, F. Sanchez, P. L. Francois, E. Delevaque, and G. Stephan, *Opt. Quantum Electron.* (to be published).
 - [13] I. M. Jauncey, L. Reekie, R. J. Mears, and C. J. Rowe, *Opt. Lett.* **12**, 164 (1987).
 - [14] W. L. Barnes, S. B. Poole, J. E. Townsend, L. Reekie, D. J. Taylor, and D. N. Payne, *IEEE J. Light. Technol.* **7**, 1461 (1989).
 - [15] W. J. Miniscalco, *IEEE J. Light. Technol.* **9**, 234 (1991).
 - [16] P. F. Wysocki, J. L. Wagener, M. J. F. Digonnet, and H. J. Shaw, *Fibre Laser Sources and Amplifiers IV*, edited by M. J. F. Digonnet and E. Snitzer [Proc. SPIE 1789 (1992)].
 - [17] J. L. Wagener, P. F. Wysocki, M. J. F. Digonnet and H. J. Shaw, in *Fibre Laser Sources and Amplifiers IV*, edited by M. J. F. Digonnet and E. Snitzer [Proc. SPIE 1789 (1992)].
 - [18] S. Pollack and D. B. Chang, *J. Appl. Phys.* **64**, 2885 (1988).
 - [19] P. Urquhart, *IEE Proc. Pt.J* **135**, 385 (1988).
 - [20] *Optical Fibre Lasers and Amplifiers*, edited by P. W. France (Blackie, Glasgow, 1991).
 - [21] E. Delevaque, T. Georges, M. Monerie, P. Lamouler, and J.-F. Bayon (unpublished).
 - [22] M. Le Flohic, P. L. Francois, J.-Y. Allain, F. Sanchez, and G. Stephan, *IEEE J. Quantum Electron.* **QE27**, 1910 (1991).
 - [23] J. C. Wright, in *Topics in Applied Physics*, edited by F. K. Fong (Springer-Verlag, New York, 1976), Vol. 15 pp. 239-295.
 - [24] F. Auzel, *Ann. Telecommun.* **24**, 199 (1969).
 - [25] J. D. Crawford, *Rev. Mod. Phys.* **63**, 991 (1991).
 - [26] G. Iooss and D. D. Joseph, in *Elementary Stability and Bifurcation Theory*, edited by J. H. Ewing, F. W. Gehring, and P. R. Halmos, Undergraduate Texts in Mathematics (Springer-Verlag, New York, 1990).
 - [27] R. J. Mears and S. R. Baker, *Opt. Quantum Electron.* **24**, 517 (1992).